Multidimensional spectroscopic probes of single molecule fluctuations

Valeri Barsegov and Shaul Mukamel
Department of Chemistry, University of Rochester, Rochester, New York 14627-0216

(Received 10 June 2002; accepted 26 August 2002)

Single photon counting time distributions obtained from single molecule photon arrival trajectories are employed in the theoretical study of multistate kinetics coupled to a two-state jump bath. The bath time scale may be extracted from statistical analysis of one- and two-point time-domain optical measurements. The amplitude and shape of the distribution of interphoton arrival times reflects bath correlations. A slow bath (relative to the kinetics) results in broad distributions of arrival times reflecting bath memory. For a fast bath, the arrival time distributions narrow around shorter times, similar to motional narrowing in frequency domain spectroscopy. The variance of either kinetic rates or equilibrium population of bath states results in asymmetry of the distribution of two photon arrival times. © *2002 American Institute of Physics.* [DOI: 10.1063/1.1515321]

I. INTRODUCTION

Single molecule (SM) measurements provide detailed information on the entire distributions of physical quantities, in contrast to bulk measurements which only yield their averages.[1–3] SM observables have distinct stochastic signatures of coupling to bath degrees of freedom.[4–7] They have been used to gain information on molecular motions, e.g., intermolecular rotation in charge conducting peptides,[8,9] protein folding,[10,11] electron transfer in DNA,[9] spectral diffusion in glasses at low temperatures (terrylene in polyethilene),[12–18] kinetics in enzymatic systems (cholesterole oxidase binding kinetics),[5] and conformational relaxation in biomolecules (DNA, tRNA).[19–23]

In many optical SM experiments, a molecule is excited by a strong continuous-wave (cw) monochromatic laser field.[12–15] The collected fluorescence photons are grouped into intervals (bins) of a certain duration (binning time). Typical observables analyzed in a cw experiment include stochastic trajectories of fluorescence intensity,[13,14] absorbtion frequency peak position,[14,17] and line shapes.[16–18] Such data have been used to probe spectral diffusion rates in the time regime between msec and sec.[16–18] An absorption frequency trajectory on a time scale of seconds can be even analyzed visually.[14,17] From such a trajectory, the two-time frequency autocorrelation function has been calculated.[24]

cw experiments on glasses at low temperatures,[12–18] were the subject of intensive theoretical investigations.[24–27] Reilly and Skinner used the Anderson–Kubo two state jump model[28,29] for the spectral diffusion of a single pentacene molecule transition frequency in *p*-terphenyl.[24] Zhao *et al.* computed the four-point correlation function and the third order response of a chromophore coupled to either a two state jump or a Brownian oscillator bath.[30] Barkai, Silbey, and Zumofen studied fluctuations of line shapes of SMs interacting with randomly distributed two-level systems by computing the distribution of moments and cumulants.[26] The same group used the two state jump model to establish the relation between line shape fluctuations of a molecule undergoing spectral diffusion and a four point correlation function of the dynamics.[25,31] Fleury *et al.* performed single photon counting (no binning) cw measurements on terrylene molecules in terphenyl crystals. Interphoton times between two consecutive photons were recorded and their histogram was used to construct the two-time fluorescence intensity autocorrelation function. The binning time which limits the time resolution is adjusted to optimize signal-to-noise ratio and in recent experiments it has been as short as μs.[12]

To observe faster fluctuations, a train of weak optical pulses separated by the time t_s has been recently applied to excite the molecule. A sequence of chronological (t) and single photon arrival times, i.e., delay times (τ) between excitation and emission events is then recorded (Fig. 1). τ is typically in the nsec regime whereas t can span a broad range of timescales from seconds down to μsec. The resulting $\{\tau,t\}$ data set forms a *photon arrival trajectory* (PAT) in which each detected photon represents a datapoint.[19,32] The separation time t is a control parameter which can be varied by changing the pulse intensity and train period to capture the characteristic bath time scale. Excitation typically occurs every 10^3 pulses of the train.

A PAT experiment is an analogue of *time domain* multiple pulse techniques ubiquitous in nonlinear spectroscopy.[33] In general, one can conduct an n-point measurement and compute an n-time histogram of arrival times $\tau_1,\ldots,\tau_n$ separated by times $t_1,\ldots,t_{n-1}$ yielding the nth order distributions of arrival times $Q_n(\tau_1,\ldots,\tau_n;t_1,\ldots,t_{n-1})$.[19,34] As n is increased, Q_n contains gradually more detailed information on the dynamics of correlations of bath variables which modulate the time scale of the kinetic process under study.[35] In this paper, we limit our discussion to one- and two-point measurements. In a one-point ($n=1$) measurement, one records a histogram of photon arrival times τ's. In a two-point ($n=2$) measurement, a set of the two photon arrival times (τ_1's and τ_2's) and their separation time t_1 is recorded. This carries information on bath dynamics on the t_1 time scale. Xie and co-workers[19] employed this technique to probe μs conformational relaxation of single DNA and tRNA molecules through fluorescence resonant energy transfer (FRET). Seidel and coworkers used the same techniques to

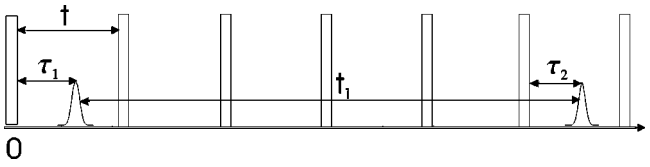

FIG. 1. One- and two-pulse PAT experiment: Interphoton times t's and arrival times τ's are obtained from time resolved single photon counting using a train of excitation pulses.

probe μs conformational dynamics of the 20-mer oligonucleotide strand of DNA.[32]

FRET experiments[23,32] involve two chromophores A and B. A absorbs a photon and undergoes a transition from the ground $|0\rangle$ to the excited $|1\rangle$ state. A photon is subsequently emitted either from A or from B, following energy transfer [Fig. 2(a)]. In a previous work,[34] we studied the arrival time distributions for the model where kinetics was coupled to a stochastic bath diffusive coordinate. We showed how PAT statistics for one- and two-point measurements of photons emitted by A can be employed to probe bath jumps on the time scale of separation times between the two emission events.

In this paper, we perform a similar analysis of emission from B for a two state jump bath to study both bath jumps and transfer kinetics [Fig. 2(a)]. If photon emission is faster than both bath jumps and transfer kinetics, the statistics of emitted photons probes bath jump timescale and one can obtain information on the distribution of kinetic rates. Coupling of kinetics to the bath makes PAT statistics non-Poissonian. By analyzing experimentally accessible PAT data, we utilize deviations of arrival time distributions from Poissonian statistics to deduce the bath time scale.

Our model is presented in Sec. II. In Sec. III we introduce the distributions of photon arrival times accessible from one- and two-point measurements. In Sec. IV we compute the arrival time distribution and in Sec. V we examine the joint distribution of two photon arrival times and employ various statistical measures for probing the dynamics of bath correlations. Our results are summarized in Sec. VI.

II. THE MODEL: ENERGY TRANSFER COUPLED TO A TWO STATE JUMP BATH

Consider reversible excitation transfer kinetics from the absorbing chromophore A to the emitting chromophore B. We assume that the system is coupled to a two state bath (α and β), which modulates its forward K^i_{ab} and backward K^i_{ba} excitation transfer rates ($i=\alpha,\beta$). The bath evolution is not affected by the kinetics.

We model the bath evolution as a stochastic Markov process and the system+bath kinetics is governed by the stochastic Liouville equation[29,36,37]

$$\dot{P}_{a,\alpha}(t)=-\sum_{b\beta} M_{a\alpha,b\beta}P_{b,\beta}(t), \tag{1}$$

with the four-dimensional population vector $\mathbf{P}(t)$

$$\mathbf{P}(t)=\begin{pmatrix}\mathbf{P}_a(t)\\ \mathbf{P}_b(t)\end{pmatrix}=\begin{pmatrix}P_{a\alpha}(t)\\ P_{a\beta}(t)\\ P_{b\alpha}(t)\\ P_{b\beta}(t)\end{pmatrix} \tag{2}$$

and

$$\mathbf{M}=\begin{pmatrix}\mathbf{K}_{ab}+\mathbf{R} & -\mathbf{K}_{ba}\\ -\mathbf{K}_{ab} & \mathbf{K}_{ba}+\mathbf{R}+\mathbf{k}\end{pmatrix}, \tag{3}$$

$\mathbf{K}$, $\mathbf{R}$, and $\mathbf{k}$ are 2×2 matrices in the α, β-space: they represent energy transfer, bath jump rates and radiative decay rates, respectively,

$$\begin{aligned}&\mathbf{K}_{ab}=\begin{pmatrix}K^\alpha_{ab} & 0\\ 0 & K^\beta_{ab}\end{pmatrix},\quad \mathbf{K}_{ba}=\begin{pmatrix}K^\alpha_{ba} & 0\\ 0 & K^\beta_{ba}\end{pmatrix},\\ &\mathbf{R}=\begin{pmatrix}R_{\alpha\beta} & -R_{\beta\alpha}\\ -R_{\alpha\beta} & R_{\beta\alpha}\end{pmatrix},\quad \mathbf{k}=\begin{pmatrix}k_b & 0\\ 0 & k_b\end{pmatrix}.\end{aligned} \tag{4}$$

Our model has three basic time scales: characteristic time scale of the bath evolution $t_B\sim 1/R=(R_{\alpha\beta}+R_{\beta\alpha})^{-1}$, kinetic time scale $t_K\sim\max\{(K^\alpha_{ab}+K^\alpha_{ba})^{-1},\ (K^\beta_{ab}+K^\beta_{ba})^{-1}\}$, and radiative lifetime $t_F\sim k_b^{-1}$.

The solution of equations (1) in Laplace domain

$$\tilde{\mathbf{P}}(z)\equiv\int_0^\infty e^{-zt}\mathbf{P}(t)dt, \tag{5}$$

reads

$$\tilde{\mathbf{P}}(z)=[z\mathbf{I}-\mathbf{M}]^{-1}\mathbf{P}(0), \tag{6}$$

where $\mathbf{I}$ is 4×4 unit matrix, $[\cdots]^{-1}$ denotes inverse of a matrix and $\mathbf{P}(0)$ is a vector representing the equilibrium distribution of states $|a,\alpha\rangle$, $|a,\beta\rangle$, $|b,\alpha\rangle$ and $|b,\beta\rangle$.

The Laplace conjugate quantity corresponding to the bulk population vector $\langle\tilde{\mathbf{P}}(z)\rangle$ can be obtained from $\tilde{\mathbf{P}}(z)$ by averaging over initial realizations of the bath

$$\langle\tilde{\mathbf{P}}(z)\rangle=\mathbf{1}[z\mathbf{I}-\mathbf{M}]^{-1}\mathbf{P}(0), \tag{7}$$

where $\mathbf{1}$ is a row vector whose elements are equal to unity. The bath state dependent population vector $\mathbf{P}(t)$ is obtained by inverse Laplace transform of Eqs. (6) and (7).

Let us now consider some limiting cases of the dynamics of $\mathbf{P}(t)$. We first write the formal solution of Eq. (1) when the system is initially in state a:

$$\begin{pmatrix}\mathbf{P}_a\\ \mathbf{P}_b\end{pmatrix}(t)=e^{-t\mathbf{M}}\begin{pmatrix}\mathbf{P}_a(0)\\ \mathbf{0}\end{pmatrix}=\mathbf{U}e^{-t\lambda}\mathbf{U}^{-1}\begin{pmatrix}\mathbf{P}_a(0)\\ \mathbf{0}\end{pmatrix}, \tag{8}$$

where λ and $\mathbf{U}$ are, respectively, the matrix of eigenvalues and eigenvectors of $\mathbf{M}$, $\mathbf{U}^{-1}$ is inverse of matrix $\mathbf{U}$ and $\mathbf{0}$ is a row with zero entries.

The eigenvalues of $\mathbf{M}$ are the roots of the secular determinant $\det(\lambda\mathbf{I}-\mathbf{M})$. Using an identity for the determinant of the square block matrix, we have[38]

$$\begin{aligned}\det(\lambda\mathbf{I}-\mathbf{M})&=\det\begin{pmatrix}\lambda\mathbf{I}-\mathbf{K}_{ab}-\mathbf{R} & -\mathbf{K}_{ba}\\ -\mathbf{K}_{ab} & \lambda\mathbf{I}-\mathbf{K}_{ba}-\mathbf{k}-\mathbf{R}\end{pmatrix}\\ &=\det(\lambda\mathbf{I}-\mathbf{K}_{ab}-\mathbf{R})\times\det(\lambda\mathbf{I}-\mathbf{K}_{ba}-\mathbf{k}-\mathbf{R}\\ &\quad-\mathbf{K}_{ab}[\lambda\mathbf{I}-\mathbf{K}_{ab}-\mathbf{R}]^{-1}\mathbf{K}_{ba}).\end{aligned} \tag{9}$$

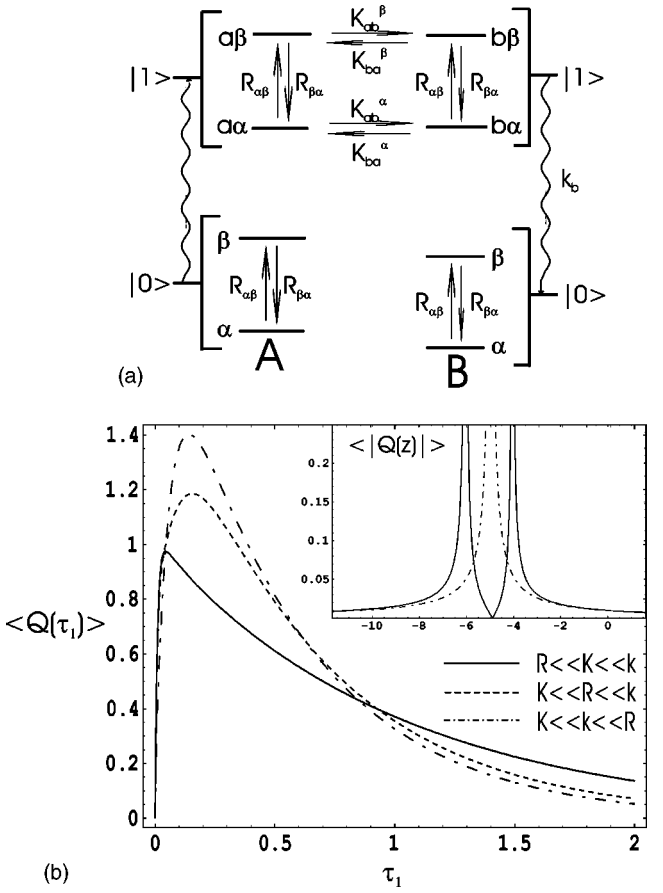

FIG. 2. (a) A two-site kinetic scheme for the creation of excitation in site A ($|0\rangle \rightarrow |1\rangle$ transition), followed by the propagation from A to B with forward $K_{ab}^{\alpha,\beta}$ and backward $K_{ba}^{\alpha,\beta}$ kinetic rates and emission of a photon from site B with rates $k_{b\alpha}$, $k_{b\beta}$. These processes are coupled to the two-state bath evolution with rates $R_{\alpha\beta}$ and $R_{\beta\alpha}$; (b) Ensemble average distribution of photon arrival times $\langle Q(\tau_1)\rangle$ vs τ_1 (in units of 10^{-7} s) for slow ($\mathbf{k}\gg\mathbf{K}\gg\mathbf{R}$, solid line), intermediate ($\mathbf{k}\gg\mathbf{R}\gg\mathbf{K}$, dashed line) and fast ($\mathbf{R}\gg\mathbf{k}\gg\mathbf{K}$, dashed and dotted line) bath. Parameters used are $k_b=1.0\times10^7\ \mathrm{s}^{-1}$, $K_{ab}^{\alpha}=4\times10^2 k_b$, $K_{ab}^{\beta}=6\times10^2 k_b$, $K_{ba}^{\alpha,\beta}=k_b$; $R_{\alpha\beta}=R_{\beta\alpha}=10^{-2}k_b$ for slow, $R_{\alpha\beta}=R_{\beta\alpha}=k_b$ for intermediate, $R_{\alpha\beta}=R_{\beta\alpha}=10^3 k_b$ for fast bath. The Laplace transform of the distribution of photon arrival times $\langle Q(z)\rangle$ for a slow and fast bath is shown in the inset. Motional narrowing is seen for the fast bath.

Let us assume that excitation return rates $\mathbf{K}_{ba}$ are small compared to $\mathbf{K}_{ab}$ and $\mathbf{k}$. Then, Eq. (9) yields

$$\det(\lambda\mathbf{I}-\mathbf{M})=\det(\lambda\mathbf{I}-\mathbf{K}_{ab}-\mathbf{R})\det(\lambda\mathbf{I}-\mathbf{k}-\mathbf{R}). \tag{10}$$

When $\mathbf{R}\ll\mathbf{K}_{ab},\mathbf{k}$, the eigenvalues of $\mathbf{M}$ are $\lambda_1=K_{ab}^{\alpha}$, $\lambda_2=K_{ab}^{\beta}$ and $\lambda_3=\lambda_4=k_b$. In this case, Eqs. (1) for populations $P_{a\alpha}(t)$, $P_{b\alpha}(t)$, and $P_{a\beta}(t)$, $P_{b\beta}(t)$ for channel α and β (see Fig. 2) are decoupled and $P_{a\alpha,b\alpha}(t)$, $P_{a\beta,b\beta}(t)$ evolve independently. However, when $\mathbf{R}\sim\mathbf{K}_{ab}$ and/or $\mathbf{R}\sim\mathbf{k}$, the two channels are coupled and $P_{a\alpha,b\alpha}(t)$, $P_{a\beta,b\beta}(t)$ mix due to bath jumps which modulates both energy transfer and photon emission rates, i.e., $\mathbf{K}_{ab}\rightarrow\mathbf{K}_{ab}+\mathbf{R}$ and $\mathbf{k}\rightarrow\mathbf{k}+\mathbf{R}$. Because the eigenvalues of $\mathbf{K}_{ab}+\mathbf{R}$ and $\mathbf{k}+\mathbf{R}$ are larger than the eigenvalues of $\mathbf{K}_{ab}$ and $\mathbf{k}$, respectively, populations $P_{b\alpha}(t)$ and $P_{b\beta}(t)$ of site B evolve on a shorter time scale and are peaked at shorter times. As a result, the distribution of photon arrival times $Q(\tau_1)\sim k_b(P_{b\alpha}(\tau_1)+P_{b\beta}(\tau_1))$ (see Sec. III), narrows at short times. Figure 2(b) in which we display the ensemble average photon arrival time distribution for a slow ($\mathbf{k}\gg\mathbf{K}\gg\mathbf{R}$), intermediate ($\mathbf{k}\gg\mathbf{R}\gg\mathbf{K}$) and fast ($\mathbf{R}\gg\mathbf{k}\gg\mathbf{K}$) bath demonstrates that the arrival time distribution shows *motional narrowing*.[29,36,37]

In the following Sections we use the population trajectory of site B ($\mathbf{P}(t)$) to compute the distributions of photon arrival times for one- and two-point measurements.

III. SINGLE- AND TWO-POINT PAT OBSERVABLES

In this Section we introduce the quantities used in the statistical analysis of one- and two-point PAT data. To analyze one-point data, we define the 2×2 conditional distribution matrix $\mathbf{Q}(\tau_1)=\{Q(\tau_1)\}_{ij}$, where $i=b\alpha,b\beta$, $j=a\alpha,a\beta$, of observing a photon arriving at τ_1 when the system is in state $b\alpha$ or $b\beta$, given that at the time of excitation $t=0$ it is in state $a\alpha$ or $a\beta$. This matrix can be constructed by taking a product of the matrix $\mathbf{k}$ of decay rates and a 2×2 block of the 4×4 matrix $[z\mathbf{I}-\mathbf{M}]^{-1}$ of Green functions corresponding to propagation of excitation from states $|a\alpha\rangle$, $|a\beta\rangle$ to states $|b\alpha\rangle$, $|b\beta\rangle$ during time τ_1, i.e.,

$$\tilde{Q}_{ij}(z)\equiv k_b\{[z\mathbf{I}-\mathbf{M}]^{-1}\}_{ij} \tag{11}$$

where $i=b\alpha,b\beta$ and $j=a\alpha,a\beta$. $\mathbf{Q}(\tau_1)$ is obtained by inverse Laplace transformation of $\tilde{\mathbf{Q}}(z)$.

Because the system can emit a photon from either state $b\alpha$ or $b\beta$, we define the joint distribution vector of photon arrival times, $\mathbf{q}(\tau_1)$, a quantity directly accessible from a one-point PAT experiment. $\mathbf{q}(\tau_1)$ can be computed by averaging $\mathbf{Q}(\tau_1)$ over the initial realizations of bath states, i.e.,

$$\mathbf{q}(\tau_1)=\begin{pmatrix} q_{b\alpha} \\ q_{b\beta}\end{pmatrix}(\tau_1)=N_1^{-1}\mathbf{Q}(\tau_1)\mathbf{w}^{\mathrm{eq}}, \tag{12}$$

where N_1 is a normalization constant

$$N_1=\int_0^\infty d\tau_1\langle\langle 1|\mathbf{Q}(\tau_1)|\mathbf{w}^{\mathrm{eq}}\rangle\rangle$$

$$\equiv\int_0^\infty d\tau_1(1\quad 1)\begin{pmatrix} Q_{b\alpha,a\alpha}(\tau_1) & Q_{b\alpha,a\beta}(\tau_1)\\ Q_{b\beta,a\alpha}(\tau_1) & Q_{b\beta,a\beta}(\tau_1)\end{pmatrix}\begin{pmatrix} P_{a\alpha}^{\mathrm{eq}}\\ P_{a\beta}^{\mathrm{eq}}\end{pmatrix} \tag{13}$$

and $\mathbf{w}^{\mathrm{eq}}$ is the equilibrium population vector

$$\mathbf{w}^{\mathrm{eq}}=\begin{pmatrix} P_{a\alpha}^{\mathrm{eq}}\\ P_{a\beta}^{\mathrm{eq}}\end{pmatrix}=\begin{pmatrix} P_{a\alpha}(0)\\ P_{a\beta}(0)\end{pmatrix}. \tag{14}$$

The macroscopic ("bulk") distribution of τ_1 is

$$\langle Q(\tau_1)\rangle=N_1^{-1}\langle\langle 1|\mathbf{Q}(\tau_1)|\mathbf{w}^{\mathrm{eq}}\rangle\rangle. \tag{15}$$

A useful statistical measure of observed PAT is given by the ensemble averaged pth moment of τ_1 which can be computed from the average histogram $\langle Q(\tau_1)\rangle$

$$\langle\tau_1^p\rangle=\int_0^\infty d\tau_1\tau_1^p\langle Q(\tau_1)\rangle. \tag{16}$$

Note that we can further construct a matrix $\mathbf{m}_p$ of the pth moments of τ_1 as $\mathbf{m}_p=N_1^{-1}\int_0^\infty d\tau_1\tau_1^p\mathbf{Q}(\tau_1)$. Note that in contrast to $\langle\tau_1^p\rangle$ which can be accessed through bulk measurements, $\mathbf{m}_p$ can only be obtained from statistical analysis on SM PAT measurements.[34]

We next turn to two-point information. Consider a process when chromophore A is excited at time t$=0$ and transfer excitation to chromophore B which emits a photon at time τ_1. Then, at later time t, A is excited again and transfers excitation to B which emits the second photon at time τ_2 after the second excitation. This process can be described by the 2×2 conditional distribution matrix with elements $Q_{ij}(\tau_1,\tau_2;t)$, of observing a pair of photons arriving, respectively, at τ_1 and τ_2 when the system is in the final state $j=b\alpha,b\beta$ and separated by time t, given that initially (at $t=0$) it was in the state $i=a\alpha,a\beta$. The matrix can be computed by taking a product of conditional probability of being excited at time $t=0$ and emitting the first photon at time τ_1 times the conditional probability representing bath evolution for time $t-\tau_1$ (when chromophores are in the ground state) times the conditional probability for the second excitation to occur at time t followed by emission of the second photon arriving at time $t+\tau_2$, i.e.,

$$\mathbf{Q}(\tau_1,\tau_2;t)=\mathbf{Q}(\tau_2)\mathbf{G}(t-\tau_1)\mathbf{Q}(\tau_1), \tag{17}$$

where $\mathbf{G}(t)$ is Green the function for our two state jump bath given in Appendix A. The joint distribution vector, $\mathbf{q}(\tau_1,\tau_2;t)$, a quantity directly accessible from two-point PAT data, can be computed from $\mathbf{Q}(\tau_1,\tau_2;t)$

$$\mathbf{q}(\tau_1,\tau_2;t)=N_2(t)^{-1}\mathbf{Q}(\tau_1,\tau_1;t)\mathbf{w}^{\mathrm{eq}}, \tag{18}$$

where $N_2(t)$ is the normalization factor

$$N_2(t)=\int_0^\infty d\tau_1\int_0^\infty d\tau_2\langle\langle 1|\mathbf{Q}(\tau_1,\tau_2;t)|\mathbf{w}^{\mathrm{eq}}\rangle\rangle. \tag{19}$$

The distribution of τ_1 and τ_2 in a bulk measurement is obtained by averaging over initial and summing over final bath states, i.e.,

$$\langle Q(\tau_1,\tau_2;t)\rangle=N_2(t)^{-1}\langle\langle 1|\mathbf{Q}(\tau_1,\tau_1;t)|\mathbf{w}^{\mathrm{eq}}\rangle\rangle. \tag{20}$$

From the moments of the conditional probability matrix $\mathbf{Q}(\tau_1,\tau_2;t)$ we can also compute a matrix of correlation functions of two photon arrival times τ_1,τ_2, i.e., $\mathbf{C}_{n_1,n_2}(t)=N_2(t)^{-1}\int_0^\infty d\tau_1\int_0^\infty d\tau_2\tau_1^{n_1}\tau_2^{n_2}\mathbf{Q}(\tau_1,\tau_2;t)$. This was done in Ref. 34 and will not be considered here.

A useful statistical measure of dynamics of bath correlations is[34,35]

$$D(\tau_1,\tau_2;t)=\langle Q(\tau_1,\tau_2;t)\rangle-\langle Q(\tau_1)\rangle\langle Q(\tau_2)\rangle. \tag{21}$$

This quantity depends on the separation time t which can be varied in the two-point experiment to capture the bath time scale.

Another useful experimental quantity that can be utilized for probing the bath time scale is the conditional probability distribution of interphoton separation times, $\mathbf{Q}(t)$. This quantity can be computed by integrating $\mathbf{Q}(\tau_1,\tau_2;t)$ over τ_1 and τ_2, i.e.,

$$\mathbf{Q}(t)=\int_0^\infty d\tau_1\int_0^\infty d\tau_2\mathbf{Q}(\tau_1,\tau_2;t). \tag{22}$$

The joint distribution vector of interphoton times $\mathbf{q}(t)$ is

$$\mathbf{q}(t)=\int_0^\infty d\tau_1\int_0^\infty d\tau_2\mathbf{q}(\tau_1,\tau_2;t), \tag{23}$$

and the ensemble averaged quantity $\langle Q(t)\rangle$ is obtained from $\langle Q(\tau_1,\tau_2;t)\rangle$ as

$$\langle Q(t)\rangle=\int_0^\infty d\tau_1\int_0^\infty d\tau_2\langle Q(\tau_1,\tau_2;t)\rangle, \tag{24}$$

$\langle Q(t)\rangle$ directly probes the decay of bath correlations.

In the coming sections we present model calculations of the above introduced quantities.

IV. SINGLE-POINT MEASUREMENTS

In this section, we compute the one-point distributions $\mathbf{Q}(\tau_1)$, $\mathbf{q}(\tau_1)$, and $\langle Q(\tau_1)\rangle$ defined in Eqs. (11)–(15). Let us first study some limiting cases of $\mathbf{Q}(\tau_1)$ when the timescales t_K, t_F and t_B are well separated.

Case I: $\mathbf{k}\gg\mathbf{K}\gg\mathbf{R}$. In this case populations of states $|a\alpha\rangle,|b\alpha\rangle$ and $|a\beta\rangle,|b\beta\rangle$ evolve independently due to absence of bath jumps, and the off-diagonal terms $Q_{b\alpha,a\beta}$ and $Q_{b\beta,a\alpha}$ are negligible. Expressions for the diagonal elements are presented in Eqs. (B1) and (B2) in Appendix B.

Case II: $\mathbf{K}\gg\mathbf{k}\gg\mathbf{R}$. As in case I, due to absence of bath jumps, populations of states $|a\alpha\rangle,|b\alpha\rangle$ and $|a\beta\rangle,|b\beta\rangle$ evolve independently. Expressions for the diagonal terms of $\mathbf{Q}(\tau_1)$ are given by same Eqs. (B1) with Eq. (B1).

When the bath is slow, the amplitude of the diagonal elements of $\mathbf{Q}(\tau_1)$ is determined in case I by transfer kinetics (K_{ab}^α, K_{ab}^α) when $t_F\ll t_K$ and in case II by fluorescence decay (k_b) when $t_F\gg t_K$. Decay rates of $\mathbf{Q}(\tau_1)$ are dominated by fluorescence decay rate constants $k_{b\alpha}$ and $k_{b\beta}$ in case I and a sum of forward and backward kinetic rates $K_{ab}^\alpha+K_{ba}^\alpha$ and $K_{ab}^\beta+K_{ba}^\beta$ in case II. In the square roots in the expressions (B2) and (B3) for $z_{1,2}^\alpha$ and $z_{1,2}^\alpha$, the cross terms $k_b(K_{ba}^\alpha-K_{ab}^\alpha)$ and $k_b(K_{ba}^\beta-K_{ab}^\beta)$ represent coupling between transfer kinetics and fluorescence decay. The dynamics of the distribution of photon arrival times does not depend on the slow bath.

Case III: $\mathbf{k}\gg\mathbf{R}\gg\mathbf{K}$. The bath undergoes jumps which mix channels α and β. As a result, $\mathbf{Q}(\tau_1)$ has off-diagonal elements. Note that due to presence of factors $(\exp[-z_1\tau_1]-\exp[-k_b\tau_1])$ and $(\exp[-z_2\tau_1]-\exp[-k_b\tau_1])$ the time profile is determined now by the competition between fluorescence decay and bath dynamics [see Eqs. (B5)]. Also, in the square roots in the expressions (B5) for z_1, z_2, a cross term $(R_{\alpha\beta}-R_{\beta\alpha})(K_{ab}^\alpha-K_{ab}^\beta)$ stands for coupling between transfer kinetics and dynamics of the bath.

Case IV: $\mathbf{K}\gg\mathbf{R}\gg\mathbf{k}$. As in case III, $\mathbf{Q}(\tau_1)$ contains the nonvanishing off-diagonal terms originating from the bath frequent jumps [see Eqs. (B6)].

In contrast to cases I and II, a fast bath in cases III and IV modulates both the amplitude and a time profile of the elements of $\mathbf{Q}(\tau_1)$ by factors that involve the forward and backward bath jump rates $R_{\alpha\beta}$ and $R_{\beta\alpha}$ and exponential factors $\exp[-(K_{ab}^\alpha+K_{ba}^\alpha)\tau_1]$ and $\exp[-(K_{ab}^\beta+K_{ba}^\beta)\tau_1]$, respectively. For a fast bath, the distribution of arrival times becomes dependent on bath jump timescale, $(R_{\alpha\beta}+R_{\beta\alpha})^{-1}$ [Eqs. (B6)]. As we shall demonstrate below, this results in shorter arrival times.

We present numerical studies of models $M1$, $M3$, $M5$, and $M7$ of a slow bath with $\mathbf{k}\gg\mathbf{K}$ ($M1$, $M3$, case I) and with

TABLE I. Numerical values of parameters used in simulations for models $M1-M14$.

Model	$R_{\alpha\beta}$, s^{-1}	$R_{\beta\alpha}$, s^{-1}	K^{α}_{ab}, s^{-1}	K^{β}_{ab}, s^{-1}	K_{ba}, s^{-1}	k, s^{-1}
$M1$	$1.0\cdot10^{5}$	$1.0\cdot10^{5}$	$1.0\cdot10^{7}$	$1.0\cdot10^{8}$	$1.0\cdot10^{7}$	$1.0\cdot10^{9}$
$M2$	$2.5\cdot10^{8}$	$2.5\cdot10^{8}$	$1.0\cdot10^{7}$	$1.0\cdot10^{8}$	$1.0\cdot10^{7}$	$1.0\cdot10^{9}$
$M3$	$1.0\cdot10^{5}$	$9.0\cdot10^{5}$	$1.0\cdot10^{7}$	$1.0\cdot10^{8}$	$1.0\cdot10^{7}$	$1.0\cdot10^{9}$
$M4$	$2.0\cdot10^{7}$	$1.8\cdot10^{8}$	$1.0\cdot10^{7}$	$1.0\cdot10^{8}$	$1.0\cdot10^{7}$	$1.0\cdot10^{9}$
$M5$	$1.0\cdot10^{5}$	$1.0\cdot10^{5}$	$1.0\cdot10^{9}$	$1.0\cdot10^{10}$	$1.0\cdot10^{9}$	$1.0\cdot10^{8}$
$M6$	$2.5\cdot10^{8}$	$2.5\cdot10^{8}$	$1.0\cdot10^{9}$	$1.0\cdot10^{10}$	$1.0\cdot10^{9}$	$1.0\cdot10^{8}$
$M7$	$1.0\cdot10^{5}$	$9.0\cdot10^{5}$	$1.0\cdot10^{9}$	$1.0\cdot10^{10}$	$1.0\cdot10^{9}$	$1.0\cdot10^{8}$
$M8$	$2.0\cdot10^{7}$	$1.8\cdot10^{8}$	$1.0\cdot10^{9}$	$1.0\cdot10^{10}$	$1.0\cdot10^{9}$	$1.0\cdot10^{8}$
$M9$	$8.0\cdot10^{5}$	$2.0\cdot10^{5}$	$5.0\cdot10^{7}$	$1.0\cdot10^{7}$	$1.0\cdot10^{7}$	$1.0\cdot10^{9}$
$M10$	$5.0\cdot10^{5}$	$5.0\cdot10^{5}$	$1.0\cdot10^{7}$	$5.0\cdot10^{7}$	$1.0\cdot10^{7}$	$1.0\cdot10^{9}$
$M11$	$2.0\cdot10^{5}$	$8.0\cdot10^{5}$	$5.0\cdot10^{7}$	$1.0\cdot10^{7}$	$1.0\cdot10^{7}$	$1.0\cdot10^{9}$
$M12$	$8.0\cdot10^{6}$	$2.0\cdot10^{6}$	$5.0\cdot10^{9}$	$1.0\cdot10^{9}$	$1.0\cdot10^{9}$	$5.0\cdot10^{7}$
$M13$	$5.0\cdot10^{6}$	$5.0\cdot10^{6}$	$1.0\cdot10^{9}$	$5.0\cdot10^{9}$	$1.0\cdot10^{9}$	$5.0\cdot10^{7}$
$M14$	$2.0\cdot10^{6}$	$8.0\cdot10^{6}$	$5.0\cdot10^{9}$	$1.0\cdot10^{9}$	$1.0\cdot10^{9}$	$5.0\cdot10^{7}$

$\mathbf{K}\gg\mathbf{k}$ ($M5$, $M7$, case II), as well as models $M2$, $M4$, $M6$ and $M8$ of a fast bath with $\mathbf{k}\gg\mathbf{K}$ ($M2$, $M4$, case III) and with $\mathbf{K}\gg\mathbf{k}$ ($M6$, $M8$, case IV). The parameters for all models are given in Table I. In models $M1$, $M2$, $M5$ and $M6$, the bath is at high temperature ($R_{\alpha\beta}=R_{\beta\alpha}$) and state β of the bath facilitates faster kinetics ($K^{\beta}_{ab}>K^{\alpha}_{ab}$). In models $M3$, $M4$, $M7$, and $M8$, the bath is at arbitrary temperature with $R_{\alpha\beta}<R_{\beta\alpha}$, but state β facilitates faster kinetics. We assume that $K^{\alpha}_{ba}=K^{\beta}_{ba}=K_{ba}$.

Simulated conditional distribution matrix elements $Q_{b\alpha,a\alpha}(\tau_1)$, $Q_{b\alpha,a\beta}(\tau_1)$, $Q_{b\beta,a\alpha}(\tau_1)$, and $Q_{b\beta,a\beta}(\tau_1)$ [see Eq. (11)] for models $M1-M8$ are presented in Figs. 3 and 4.

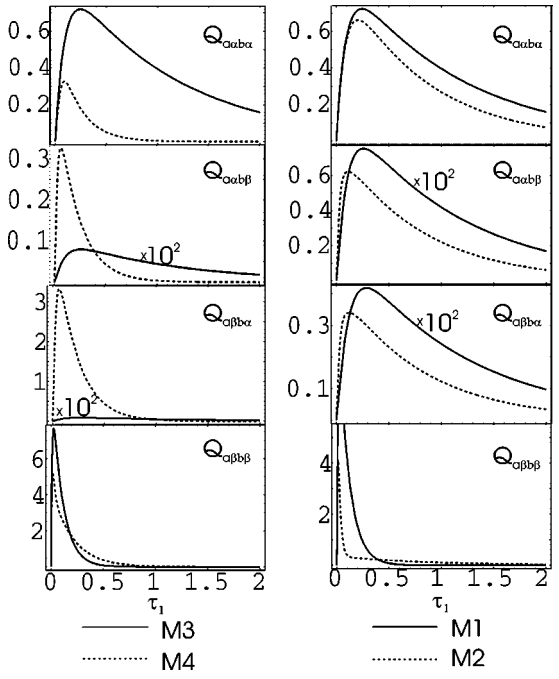

FIG. 3. From top to bottom: elements $Q_{a\alpha,b\alpha}(\tau_1)$, $Q_{a\alpha,b\beta}(\tau_1)$, $Q_{a\beta,b\alpha}(\tau_1)$ and $Q_{a\beta,b\beta}(\tau_1)$ of the photon arrival time density $\mathbf{Q}(\tau_1)$ vs τ_1 (in units of 10^{-7} s) for models $M1$ and $M2$ (right panels), and models $M3$ and $M4$ (right panels). Solid (dashed) lines correspond to models $M1$, $M3$ ($M2$, $M4$) of a slow (fast) bath.

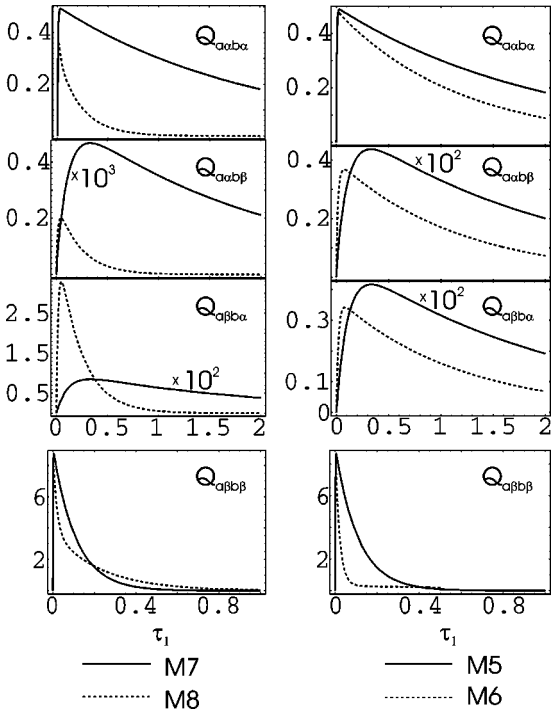

FIG. 4. From top to bottom: elements $Q_{a\alpha,b\alpha}(\tau_1)$, $Q_{a\alpha,b\beta}(\tau_1)$, $Q_{a\beta,b\alpha}(\tau_1)$ and $Q_{a\beta,b\beta}(\tau_1)$ of the photon arrival time density $\mathbf{Q}(\tau_1)$ vs τ_1 (in units of 10^{-7} s) for models $M5$ and $M6$ (right panels), and models $M7$ and $M8$ (right panels). Solid (dashed) lines correspond to models $M1$, $M3$ ($M2$, $M4$) of a slow (fast) bath.

We first study the conditional distribution $\mathbf{Q}(\tau_1)$ for cases I and III (Fig. 3). When a slow bath is at high temperature and one of the two bath states facilitates faster kinetics ($K^{\beta}_{ab}>K^{\alpha}_{ab}$, model $M1$), the "diagonal" paths $a\alpha\rightarrow a\alpha$ and $b\beta\rightarrow b\beta$ dominate over the off-diagonal paths $a\alpha\rightarrow b\beta$ and $b\beta\rightarrow a\alpha$, and the diagonal elements $Q_{b\alpha,a\alpha}(\tau_1)$ and $Q_{b\beta,a\beta}(\tau_1)$ contribute primarily to the distribution $\mathbf{Q}(\tau_1)$ (solid lines in right panels in Fig. 3). Here, the contribution from single-transition evolution paths $a\alpha\rightarrow b\beta$, $a\beta\rightarrow b\alpha$ to the off-diagonal elements of $\mathbf{Q}(\tau_1)$ are negligible (compare, e.g., the magnitude of $Q_{b\alpha,a\beta}$ and $Q_{b\beta,a\alpha}$ with the magnitude of $Q_{b\alpha,a\alpha}$ and $Q_{b\beta,a\beta}$). However, since state β of the bath facilitates faster kinetics, $Q_{b\beta,a\beta}$ has greater amplitude compared to $Q_{b\alpha,a\alpha}$. When the bath is fast, (model $M2$), its jumps become more probable and a share of the off-diagonal elements originating from single-transition paths grows at the expence of the diagonal ones (dashed lines in right panels in Fig. 3).

When a fast bath is at arbitrary temperature ($R_{\alpha\beta}<R_{\beta\alpha}$), but state β facilitates faster kinetics ($K^{\beta}_{ab}>K^{\alpha}_{ab}$, model $M3$), contributions from the off-diagonal paths become negligible and the distribution $\mathbf{Q}(\tau_1)$ is maximized by a single element $Q_{b\beta,a\beta}$ representing the bath evolution involving state β (solid lines in left panels in Fig. 3). As in $M1$, a share of the off-diagonal elements $Q_{b\alpha,a\beta}$, $Q_{b\beta,a\alpha}$ is small (bath jumps are still rare). However, when bath is fast (model $M4$), jumps occur more often, and a share of the off-diagonal elements grows (dashed lines in left panels in Fig. 3). In contrast to model $M2$, $Q_{b\alpha,a\beta}$ of model $M4$ has greater magnitude compared to $Q_{b\beta,a\alpha}$, since path $a\alpha\rightarrow b\beta$ be-

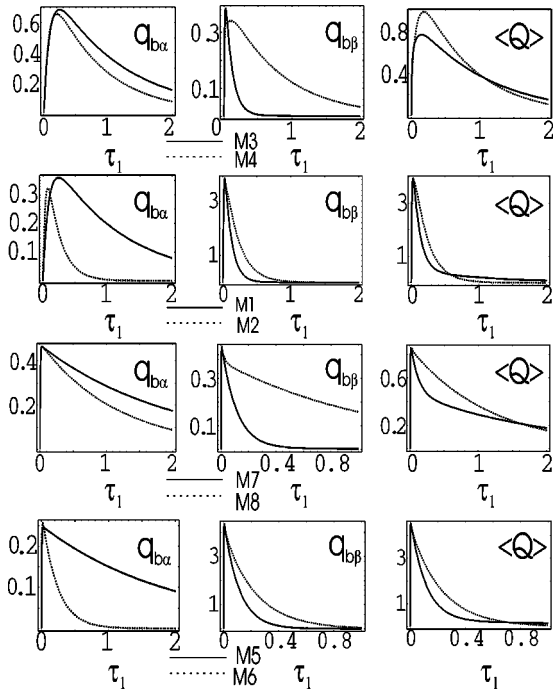

FIG. 5. From top to bottom: Components $q_{b\alpha}(\tau_1)$ (left panels), $q_{b\beta}(\tau_1)$ (middle panels) of the joint disitribution vector $\mathbf{q}(\tau_1)$ and the ensemble average distribution $\langle Q(\tau_1)\rangle$ (right panels) vs τ_1 (in units of 10^{-7} s) for models $M3$, $M4$ (top panels), $M1$, $M2$ (upper middle panels), $M7$, $M8$ (lower middle panels) and $M5$, $M6$ (bottom panels). Solid lines represent models $M1$, $M3$, $M5$, and $M7$ of a slow bath; dashed lines correspond to models $M2$, $M4$, $M6$, and $M8$ of a fast bath.

comes probabilistically more favorable than path $a\beta \rightarrow b\alpha$.

The conditional distribution $\mathbf{Q}(\tau_1)$ for cases II and IV is displayed in Fig. 4. We see that the corresponding elements of the distribution $\mathbf{Q}(\tau_1)$ computed, respectively, for models $M5$, $M6$ (right panels) and $M7$, $M8$ (left panels) exhibit similar tendencies as those of models $M1$, $M2$ and $M3$, $M4$ namely, negligible (models $M5$, $M7$) and almost equal (models $M6$, $M8$) contributions from the off-diagonal elements $Q_{b\alpha,a\beta}$ and $Q_{b\beta,a\alpha}$ compared to their diagonal counterparts $Q_{b\alpha,a\alpha}$ and $Q_{b\beta,a\beta}$. Notice, however, that the distribution $\mathbf{Q}(\tau_1)$ of models $M5$, $M6$, $M7$, and $M8$ are characterized by shorter most probable photon arrival times.

The quantities defined in Eqs. (12)–(15), can be computed from a histogram of arrival time obtained from experimental PAT data and can be further utilized to construct several quantities sensitive to bath dynamics. For example, if the characteristic bath time scale excedes t, one obtains a single PAT from a single one-point experiment on a SM, resulting in just one element ($q_{b\alpha}$ or $q_{b\beta}$) of the joint probability vector $\mathbf{q}(\tau_1)$. If PAT data are collected from many experimental runs on many molecules, one obtains the macroscopic ("bulk") distribution of τ_1.

$q_{b\alpha}$ and $q_{b\beta}$ and $\langle Q(\tau_1)\rangle$ for models $M1-M8$ are displayed in Fig. 5. The dynamics of various elements of the distribution $\mathbf{Q}(\tau_1)$ is reflected in a time profile of the joint distribution components $q_{b\alpha}$ and $q_{b\beta}$ (left and middle panels in Fig. 5) for models $M3$, $M4$ (top panels), $M1$, $M2$ (upper middle panels) and models $M7$, $M8$ (lower middle panels), $M5$, $M6$ (bottom panels). Since state β facilitates faster kinetics, $q_{b\beta}$ has shorter most probable arrival time compared to $q_{b\alpha}$ in models $M1-M4$ where transfer kinetics is the rate determining step. This effect is less pronounced for models $M5-M8$ where emission of a photon determines the overall rate of a process. Due to this coupling of kinetics to the bath evolution, paths involving state β are kinetically more favorable, and models $M2$, $M4$, $M6$, $M8$ of a fast bath all have a decreased share of $q_{b\alpha}$ and an increased share of $q_{b\beta}$ compared to models $M1$, $M3$, $M5$, $M7$ of a slow bath.

The ensemble-averaged distribution of arrival times $\langle Q(\tau_1)\rangle$ for models $M1-M8$ is presented in the right column in Fig. 5. Detailed microscopic information on contributions from various evolution paths to the distribution $\mathbf{Q}(\tau_1)$ is completely lost in the bulk quantity $\langle Q(\tau_1)\rangle$, and we are left with a highly averaged picture. Although a fast bath hardly changes the peak position of the most probable arrival time (compared to a slow bath), it eliminates long tails of $\langle Q(\tau_1)\rangle$ by putting more weight on shorter arrival times. In analogy with frequency domain spectroscopy, due to coupling of transfer kinetics to the bath, the distribution of photon arrival times exhibits motional narrowing.

V. TWO-POINT MEASUREMENTS

In the previous section we found that when $\mathbf{R} \ll \mathbf{K}$, the joint distribution vector $\mathbf{q}(\tau_1)$ corresponding to a one-point measurement is not sensitive to the bath dynamics [see Eqs. (B1)–(B3), cases I and II]. This is when two-point measurements become most valuable. In this section, we compute the joint distributions $\mathbf{Q}(\tau_1,\tau_2;t)$, $\mathbf{q}(\tau_1,\tau_2;t)$ and $\langle Q(\tau_1,\tau_2;t)\rangle$ of two-photon arrival times.

Let us first analyze the contributions to the joint distribution vector $\mathbf{q}(\tau_1,\tau_2;t)$ from various evolution paths. Although this quantity depends explicitly on the final state of the system when the second photon is emitted, $\mathbf{q}(\tau_1,\tau_2;t)$ involves contributions from 16 paths $i \rightarrow j \rightarrow k \rightarrow l$, where $i,k = a\alpha, a\beta$ and $j,l = b\alpha, b\beta$. Here i is state of the system when it absorbs the first photon, j is a state when the first photon is emitted, k is a state of the system corresponding to the second excitation and l denotes a state corresponding to emission of the second photon. These paths are summarized in Table II.

There are two "diagonal" paths 1 and 2, six single-transition paths 3–8, six two-transition paths 9–14 and two three-transition paths 15 and 16. Depending on the bath evolution timescale t_B and separation time t, the time profile of elements of the distribution $\mathbf{q}(\tau_1,\tau_2;t)$ as well as the average quantity $\langle Q(\tau_1,\tau_2;t)\rangle$ is determined by the interplay of weighted contributions from the most dominant paths.

We shall study the evolution of correlations of bath variables and present the joint distribution of two photon arrival times only for models of a slow bath (cases I and II) with kinetics (models $M9$, $M10$, and $M11$) and decay of fluorescence (models $M12$, $M13$, and $M14$) as a rate limiting step. In models $M10$ and $M13$, the bath is at high temperature and state β facilitates faster kinetics. In models $M9$, $M12$, $M11$, and $M14$ the bath is at arbitrary temperature. In model $M9$, $M12$ state $a\alpha$ is less equilibrium populated but facilitates faster kinetics. In models $M11$ and $M14$ state $a\alpha$ is both more equilibrium populated and facilitating faster kinetics.

TABLE II. System evolution paths contributing to the joint distributions $\mathbf{Q}(\tau_1,\tau_2;t)$, $\mathbf{q}(\tau_1,\tau_2;t)$ and $\langle Q(\tau_1,\tau_2;t)\rangle$.

Path	i	j	k	l
1	$a\alpha$	$b\alpha$	$a\alpha$	$b\alpha$
2	$a\beta$	$b\beta$	$a\beta$	$b\beta$
3	$a\alpha$	$b\alpha$	$a\alpha$	$b\beta$
4	$a\alpha$	$b\alpha$	$a\beta$	$b\beta$
5	$a\alpha$	$b\beta$	$a\beta$	$b\beta$
6	$a\beta$	$b\beta$	$a\beta$	$b\alpha$
7	$a\beta$	$b\beta$	$a\alpha$	$b\alpha$
8	$a\beta$	$b\alpha$	$a\alpha$	$b\alpha$
9	$a\alpha$	$b\alpha$	$a\beta$	$b\alpha$
10	$a\alpha$	$b\beta$	$a\alpha$	$b\beta$
11	$a\alpha$	$b\beta$	$a\beta$	$b\alpha$
12	$a\beta$	$b\beta$	$a\alpha$	$b\beta$
13	$a\beta$	$b\alpha$	$a\beta$	$b\beta$
14	$a\beta$	$b\alpha$	$a\alpha$	$b\beta$
15	$a\beta$	$b\alpha$	$a\beta$	$b\alpha$
16	$a\alpha$	$b\beta$	$a\alpha$	$b\beta$

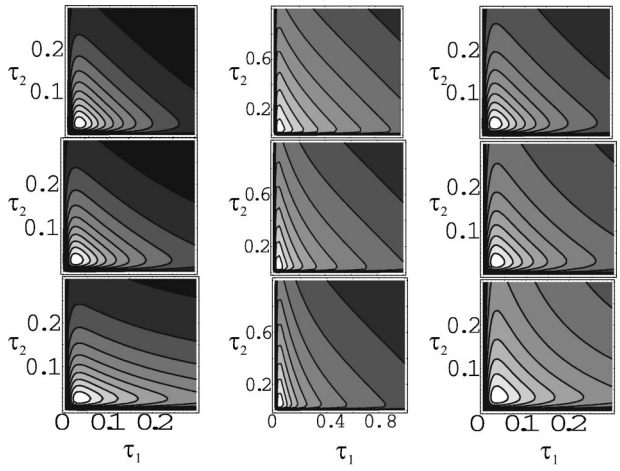

FIG. 7. Contour plots of the calculations of Fig. 6.

In Fig. 6 we present three-dimensional plots of the components $q_{b\alpha}(\tau_1,\tau_2;t)$ (left panels) and $q_{b\beta}(\tau_1,\tau_2;t)$ (middle panels) of the distribution $\mathbf{q}(\tau_1,\tau_2;t)$ for model $M9$ for three values of separation time t: (a) When bath jumps are improbable, $t\ll t_B$, (b) few bath jumps, $t\sim t_B$ and (c) many jumps (bath is in equilibrium), $t\gg t_B$. Corresponding contour plots are presented, respectively, in Fig. 7. The same calculations are repeated for model $M10$ (Figs. 8 and 9) and for model $M11$ (Figs. 10 and 11).

Because in model $M9$, state $a\alpha$ is less populated but facilitates faster kinetics and because individual photon emission events are controlled by $Q_{b\alpha,a\alpha}$ and $Q_{b\beta,a\beta}$ of Eqs. (B1) directly proporional to, respectively, K^{α}_{ab} and K^{α}_{ab} and no jump occur during separation time $t\ll t_B$ (top panels), $q_{b\alpha}$ and $q_{b\beta}$ are dominated by the diagonal paths 1 and 2, respectively. As a result, $q_{b\alpha}$ is larger than $q_{b\beta}$ (Fig. 6) and shorter most probable arrival times. Since for $t\ll t_B$ the first and second photon emission events are strongly correlated (memory, non-Poissonian signatures), contour plots for $q_{b\alpha}$ and $q_{b\beta}$ (Fig. 7) are symmetric with respect to the interchange of τ_1 and τ_2.

When $t\sim t_B$ (middle panels), few bath jumps occur and correlations between emission events decay. $q_{b\alpha}$ and $q_{b\beta}$ are dominated by single-transition paths 3–8, respectively. Because of this, $q_{b\alpha}$ is controlled by a process when the first and the second photon is emitted from state $b\beta$ and $b\alpha$, respectively, whereas $q_{b\beta}$ is controlled by a process when the first and the second photon is emitted from state $b\alpha$ and $b\beta$. As a result, the amplitude of $q_{b\alpha}$ ($q_{b\beta}$) decays (grows), and a time profile of $q_{b\alpha}$ and $q_{b\beta}$ is now longer τ_1-shorter τ_2 and shorter τ_1-longer τ_2, respectively. As the joint probability grows along the τ_1- and τ_2-axes at the expence of the diag-

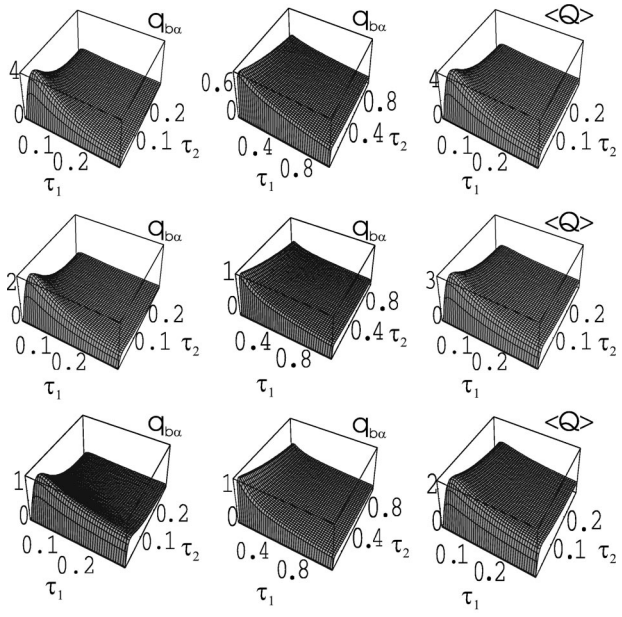

FIG. 6. The joint probability distribution: $q_{b\alpha}(\tau_1,\tau_2;t)$ (left panels), $q_{b\beta}(\tau_1,\tau_2;t)$ (middle panels) and $\langle Q(\tau_1,\tau_2;t)\rangle$ (right panels) vs τ_1 and τ_2 (in units of 10^{-7} s) for model $M9$ of case I for $t=3.0\times10^{-7}$ s^{-1} (top), $t=1.0\times10^{-8}$ s^{-1} (middle) and $t=1.0\times10^{-9}$ s^{-1} (bottom).

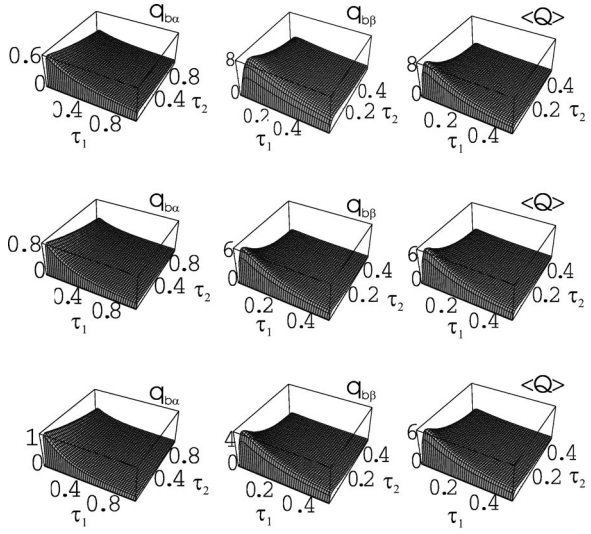

FIG. 8. The joint probability distribution: $q_{b\alpha}(\tau_1,\tau_2;t)$ (left panels), $q_{b\beta}(\tau_1,\tau_2;t)$ (middle panels) and $\langle Q(\tau_1,\tau_2;t)\rangle$ (right panels) vs τ_1 and τ_2 (in units of 10^{-7} s) for model $M10$ of case I for $t=3.0\times10^{-7}$ s^{-1} (top), $t=1.0\times10^{-8}$ s^{-1} (middle) and $t=1.0\times10^{-9}$ s^{-1} (bottom).

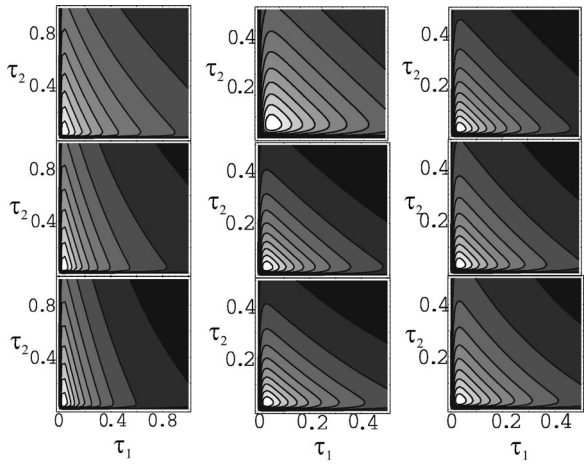

FIG. 9. Contour plots of the calculations of Fig. 8.

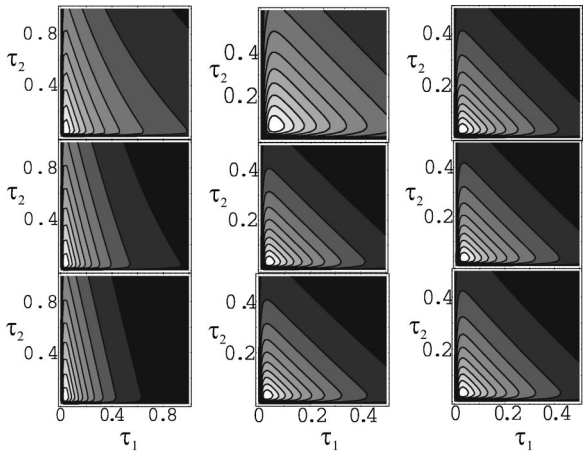

FIG. 11. Contour plots of the calculations of Fig. 10.

onal features, contour lines become more convex inward indicating decay of bath correlations. When $t \gg t_B$ (bottom panels), this is even more pronounced.

In model $M10$, states $a\alpha$ and $a\beta$ are equally populated, but state $a\beta$ facilitates faster kinetics. Here, $q_{b\alpha}$ is of negligible amplitude compared to $q_{b\beta}$ (Fig. 8) for $t \ll t_B$, because a contribution from path 2 dominates over that of path 1, and a time profile of $q_{b\alpha}$ ($q_{b\beta}$) is long τ_1, τ_2 (short τ_1, τ_2). When $t \sim t_B$, due to coupling of kinetics to the bath, as in model $M9$ single-transition paths dominate both $q_{b\alpha}$ and $q_{b\beta}$. The amplitude of $q_{b\alpha}$ therefore grows at the expense of $q_{b\beta}$, and as $q_{b\alpha}$ ($q_{b\beta}$) is controlled by shorter first and longer second (longer first and shorter second) photon emission, a time profile of $q_{b\alpha}$ and $q_{b\beta}$ becomes shorter τ_1-longer τ_2 and longer τ_1-shorter τ_2, respectively. As we go to the limit of long separation time, this tendency becomes more prominent. When $t \gg t_B$, $q_{b\alpha}$ and $q_{b\beta}$ are of comparable amplitude, and contour plots for both $q_{b\alpha}$ and $q_{b\beta}$ become convex in, signifying decay of correlations between the first and second photon emission processes (see Fig. 9).

In model $M11$ state $a\beta$ is now both more populated at equilibrium and facilitates faster kinetics. As a result, $q_{b\beta}$ dominates over $q_{b\alpha}$ for all separation times (compare, e.g., the magnitude of $q_{b\beta}$ and $q_{b\alpha}$ in Fig. 10) as contributions from evolution paths involving states $a\alpha$ and $b\alpha$ become negligible. Note that time profile of both $q_{b\alpha}$ and $q_{b\beta}$ does not change with t and is longer τ_1, τ_2 for $q_{b\alpha}$, while shorter τ_1, τ_2 for $q_{b\beta}$.

Let us now turn to models $M12$ (Fig. 12), $M13$ (Fig. 13), and $M14$ (Fig. 14). We have simulated three-dimensional plots of $q_{b\alpha}(\tau_1, \tau_2; t)$ (left panels) and $q_{b\beta}(\tau_1, \tau_2; t)$ (middle panels) of the distribution $\mathbf{q}(\tau_1, \tau_2; t)$ for two values of sepa-

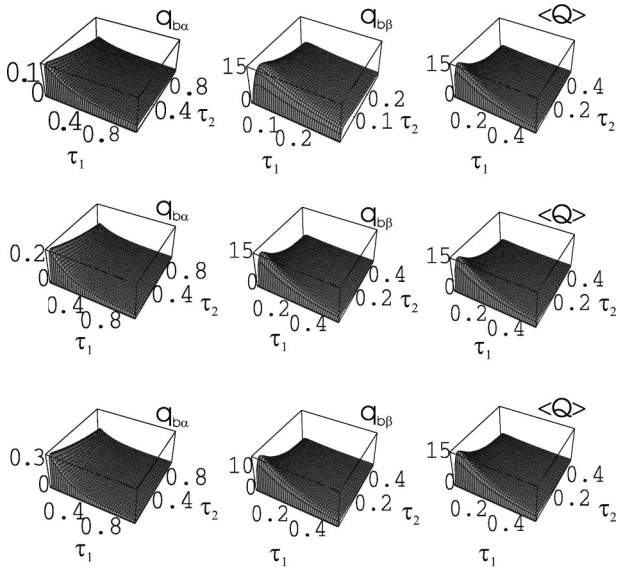

FIG. 10. The joint probability distribution: $q_{b\alpha}(\tau_1, \tau_2; t)$ (left panels), $q_{b\beta}(\tau_1, \tau_2; t)$ (middle panels) and $\langle Q(\tau_1, \tau_2; t)\rangle$ (right panels) vs τ_1 and τ_2 (in units of 10^{-7} s) for model $M11$ of case I for $t = 3.0 \times 10^{-7}$ s^{-1} (top), $t = 1.0 \times 10^{-8}$ s^{-1} (middle) and $t = 1.0 \times 10^{-9}$ s^{-1} (bottom).

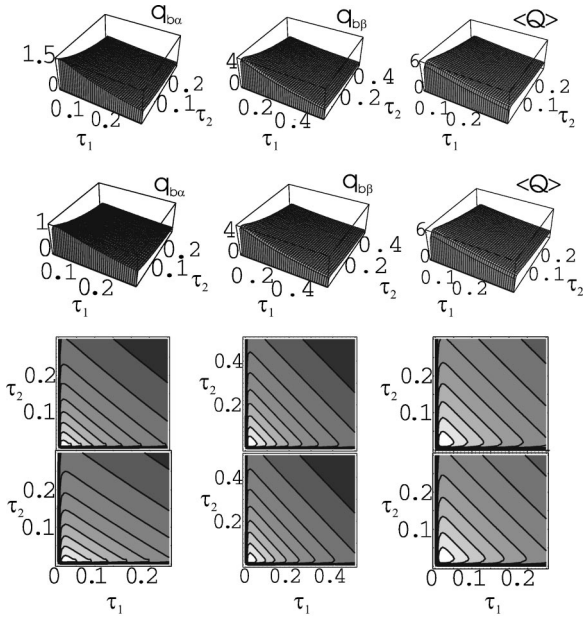

FIG. 12. Three-dimensional plots (top and upper middle panels) and contour plots (lower middle and bottom panels) of the joint probability distribution: $q_{b\alpha}(\tau_1, \tau_2; t)$ (left panels), $q_{b\beta}(\tau_1, \tau_2; t)$ (middle panels) and $\langle Q(\tau_1, \tau_2; t)\rangle$ (right panels) vs τ_1 and τ_2 (in units of 10^{-7} s) for model $M12$ of case II for $t = 1.0 \times 10^{-7}$ s^{-1} (top and lower middle panels) and $t = 2.0 \times 10^{-8}$ s^{-1} (upper middle and bottom panels).

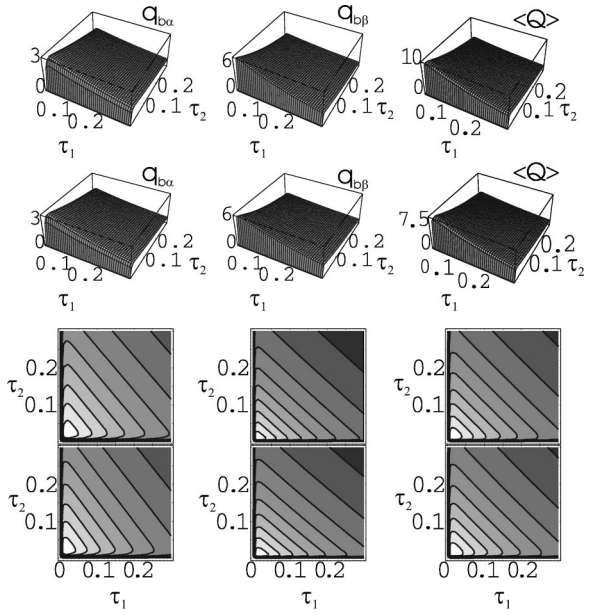

FIG. 13. Three-dimensional plots (top and upper middle panels) and contour plots (lower middle and bottom panels) of the joint probability distribution: $q_{b\alpha}(\tau_1,\tau_2;t)$ (left panels), $q_{b\alpha}(\tau_1,\tau_2;t)$ (middle panels) and $\langle Q(\tau_1,\tau_2;t)\rangle$ (right panels) vs τ_1 and τ_2 (in units of 10^{-7} s) for model $M13$ of case II for $t=1.0\times10^{-7}$ s^{-1} (top and lower middle panels) and $t=2.0\times10^{-8}$ s^{-1} (upper middle and bottom panels).

ration time, when $t\ll t_B$ and $t\gg t_B$ (top and upper middle panels). The contour plots corresponding to these models are presented in lower middle and bottom panels.

In contrast to models $M9$, $M10$, and $M11$, in models $M12$, $M13$, and $M14$, the amplitude of $q_{b\alpha}$ and $q_{b\beta}$ is determined primarily by **k** [see Eqs. (B1) and (B3)] and since in our simulation we took equal radiative decay rate constants for both channels α and β, the amplitude of $q_{b\alpha}$ and $q_{b\beta}$ is controlled by the weight of dominant paths contributing to $q_{b\alpha}$ and $q_{b\beta}$, determined by both equilibrium population of states $a\alpha$, $a\beta$ as well as evolution of the bath during time t. For instance, in model $M12$ $q_{b\beta}$ has larger amplitude compared to $q_{b\alpha}$ for both $t\ll t_B$ and $t\gg t_B$. When $t\gg t_B$, the bath approaches equilibrium before the second excitation occurs, and the amplitude of $q_{b\alpha}$ and $q_{b\beta}$ is determined solely by the equilibrium population of states $a\alpha$ and $a\beta$. As a result, $q_{b\alpha}$ grows at the expense of $q_{b\beta}$. The latter is dominated by a contribution from diagonal path 2 for $t\ll t_B$ but involves contributions from paths 3–5 for $t\gg t_B$. On the other hand, $q_{b\alpha}$ is dominated by path 1 for $t\ll t_B$ and involves contributions from paths 6–8. Because of this, time profile of $q_{b\beta}$ and $q_{b\alpha}$ is, respectively, long τ_1,τ_2 and short τ_1,τ_2 for $t\ll t_B$, but shorter τ_1-longer τ_2 and longer τ_1-shorter τ_2 for $t\gg t_B$.

In model $M13$, equilibrium populations of states $a\alpha$ and $a\beta$ are equal, and the amplitudes of $q_{b\alpha}$ and $q_{b\beta}$ are almost same for both $t\ll t_B$ and $t\gg t_B$. Since in this model $K_{ab}^{\alpha}<K_{ab}^{\beta}$, time profiles of $q_{b\alpha}$ and $q_{b\beta}$ are reversed ($q_{b\beta}$ and $q_{b\alpha}$ are short τ_1, τ_2-like and long τ_1, τ_2-like for $t\ll t_B$ and longer τ_1-shorter τ_2 and shorter τ_1-longer τ_2 for $t\gg t_B$). In model $M14$, because both $R_{\beta\alpha}<R_{\alpha\beta}$ and $K_{ab}^{\alpha}<K_{ab}^{\beta}$, $q_{b\beta}$ completely dominates over $q_{b\alpha}$ (compare, e.g., the amplitude of $q_{b\alpha}$ and $q_{b\beta}$).

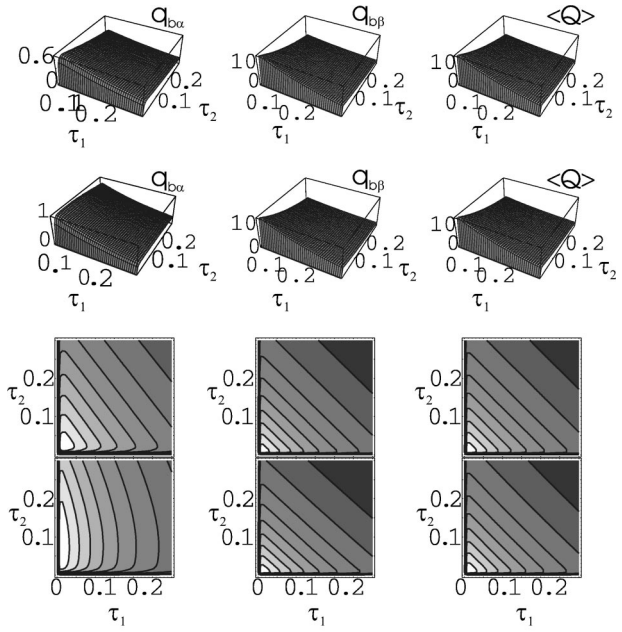

FIG. 14. Three-dimensional plots (top and upper middle panels) and contour plots (lower middle and bottom panels) of the joint probability distribution: $q_{b\alpha}(\tau_1,\tau_2;t)$ (left panels), $q_{b\beta}(\tau_1,\tau_2;t)$ (middle panels) and $\langle Q(\tau_1,\tau_2;t)\rangle$ (right panels) vs τ_1 and τ_2 (in units of 10^{-7} s) for modified model $M14$ of case II for $t=1.0\times10^{-7}$ s^{-1} (top and lower middle panels) and $t=2.0\times10^{-8}$ s^{-1} (upper middle and bottom panels).

Let us now turn to the ensemble-averaged quantity $\langle Q(\tau_1,\tau_2;t)\rangle$. Clearly, since this is an equilibrium population weighted superposition of $q_{b\alpha}$ and $q_{b\beta}$, it contains more averaged information on elementary processes involved (right panels in Figs. 6, 8, 10, and 12–14). For example, $\langle Q(\tau_1,\tau_2;t)\rangle$ carries information on the most probable pair of arrival times $\{\tau_1,\tau_2\}$ and allows to compute the two-time correlation function of τ_1 and τ_2

$$\langle \tau^{n_1}(0)\tau^{n_2}(t)\rangle \equiv \int_0^\infty d\tau_1 \int_0^\infty d\tau_2 \tau_1^{n_1}\tau_2^{n_2}\langle Q(\tau_1,\tau_2;t)\rangle. \tag{25}$$

By comparing contour plots of $\langle Q(\tau_1,\tau_2;t)\rangle$ for several separation times, we gain an insight into dynamics of bath correlations (lower middle and bottom panels in Figs. 7, 9, 11, and 12–14). At shorter separation times, in models $M9-M11$ with kinetics controlling the overall rate of emission of a photon, contour lines are straight whereas convex inward at longer times. This implies that due to coupling of kinetics to the bath, at shorter separation times when bath jumps are rare, emission events of the first and second photon are correlated (memory effect), and $\langle Q(\tau_1,\tau_2;t)\rangle$ is different from a product of individual distributions, i.e., $\langle Q(\tau_1,\tau_2;t)\rangle-\langle Q(\tau_1)\rangle\langle Q(\tau_2)\rangle\neq 0$ (non-Poissonian signature). When $t\gg t_B$, as the bath approaches equilibrium and loses memory of its initial state, correlations between emission events are irretrievably lost implying their statistical independence, i.e., the joint distribution of arrival times becomes bi-Poissonian (i.e., Poissonian with respect to both τ_1 and τ_2).

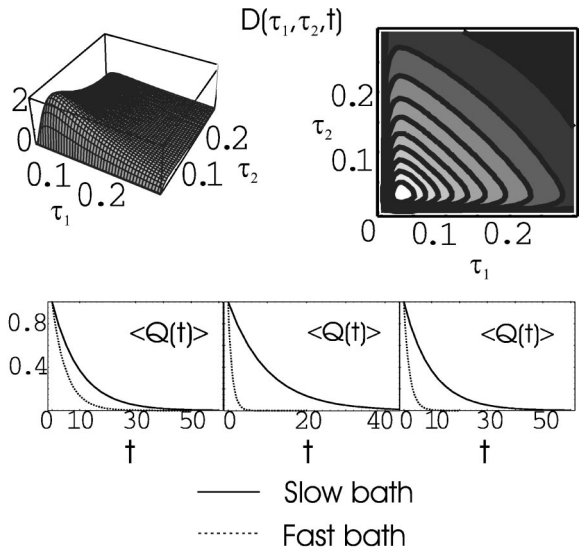

FIG. 15. Top: Three-dimensional plot (left) and contour plot (right) of the difference $D(\tau_1,\tau_2;t)$ vs τ_1 and τ_2 (in units of 10^{-7} s) for model $M9$ for $t=3.0\times10^{-7}$ s^{-1}. Bottom: $\langle Q(t)\rangle$ for models $M10$ (left panel), $M9$ (middle panel) and $M11$ (right panel). Parameters used for a slow bath (solid lines) are accumulated in Table I. Parameters used for a fast bath models $M9'$, $M10'$, and $M11'$ (dashed lines) are same as those for a slow bath except that $R_{\alpha\beta}$ and $R_{\beta\alpha}$ have been multiplied by a factor of ten.

Indeed, using the properties of $\mathbf{G}(t)$ for a two-state jump bath given in Appendix A, one can show that when $t \gg (R_{\alpha\beta}+R_{\beta\alpha})^{-1}$, $\langle Q(\tau_1,\tau_2;t)\rangle$ is factorized

$$\langle Q(\tau_1,\tau_2;t)\rangle \rightarrow \langle Q(\tau_1)\rangle\langle Q(\tau_2)\rangle. \tag{26}$$

This limiting property allows us to study the dynamics of correlations in variables of the bath by defining statistical measures sensitive to the characteristic bath time scale [see, e.g., Eq. (21)].

In contrast to models $M9-M11$, $\langle Q(\tau_1,\tau_2;t)\rangle$ of models $M12-M14$ does not change with t (compare, e.g., the amplitude of surfaces in the right panels in Figs. 12–14 for $t \ll t_B$ and $t \gg t_B$) and contour lines remain straight at all times, indicates absence of bath correlations. Indeed, in models $M12-M14$ radiative decay is not coupled to the bath, rendering evolution paths ending in state $b\alpha$ indistinguishable from those ending in state $b\beta$.

We have simulated $D(\tau_1,\tau_2;t)$ [Eq. (21)] for models $M9-M11$. Because the two-dimensional surfaces and contour plots of $D(\tau_1,\tau_2;t)$ for these models and various separation times look qualitatively similar, in Fig. 15 we present surfaces and contour plots only for model $M9$ for $t \ll t_B$. As t increases, the amplitude of $D(\tau_1,\tau_2;t)$ decays implying decay of bath correlations (not shown). Convex contour lines indicate the presence of correlations between the first and second photon emission events. The contour plots are *not* symmetric with respect to the interchange of τ_1 and τ_2, since the lines of equal probability are stretched more along τ_1-axis compared to τ_2-axis. This can be rationalized by recalling that in this model kinetics is a rate determining step and that state $a\alpha$ is more frequently visited (equilibrium populated), whereas state $a\beta$ facilitates faster transfer kinetics. Because of this, the first photon is emitted (on average) from state $b\alpha$ and is emitted faster compared to the second photon emitted (on average) from state $b\beta$.

We have simulated $\langle Q(t)\rangle$ for models $M9-M11$ for a slow and fast bath. The normalized quantity $\langle Q(t)\rangle/\langle Q(0)\rangle$ is presented in Fig. 15 (bottom panels). For all models a fast bath curve lies below a corresponding slow bath curve. Due to more frequent jumps in models $M9$ and $M11$, correlations live shorter compared to model $M10$.

VI. CONCLUSIONS

In this paper we studied the distribution of kinetic rates in a system where energy transfers between the site A in which excitation is created by weak optical pulse and the site B from which a fluorescence photon is emitted. The transfer kinetics is coupled to a two-state jump bath which is not affected by kinetics.

We have demonstrated how the bath evolution and the distribution of kinetic rates may be studied using one- and two-point PAT data. A statistical analysis yields physical quantities related to the dynamics of bath correlations: The photon arrival time distribution which is directly accessible through analysis of one-point PAT data was computed,[34] the distributions of arrival times for two photons, etc. These quantities can be obtained from experimental histograms of PAT data. Using one-and two-photon arrival time distributions, we examined several measures that can be employed in the statistical analysis of one- and two-point PAT data to probe dynamics of bath correlations and extract the characteristic bath evolution time scale.

The arrival time distribution provides information on the distribution of kinetic rates; the joint distribution of arrival times of two adjacent photons probes both the distribution of kinetic rates and stochastic bath jumps on the time scale of separation time. Similar information can be obtained by looking at emission from chromophore A. However, the present study of emission from B is a good starting point for an extended kinetic model where excitation transfers among n chromophores $A_1,A_2,\ldots,A_n$. This model may apply to electron transfer in DNA,[8] or hole transfer in peptides.[9]

Due to coupling of the excitation transfer process to the bath, the arrival time distributions exhibit interesting types of static and dynamic behaviors, caused by changing weights of the relevant bath evolution paths. This can only be observed through SM measurements; simulated bulk quantities (corresponding to optical measurements on the bulk) yield a highly averaged picture where the entire spectrum of static and dynamic behaviors is averaged out.

Coupling of the kinetics to a slow (compared to kinetic timescale and radiative lifetime) bath results in longer (on average) photon arrival times. The distribution of arrival times exhibits long tails indicating the presence of bath memory to its initial state. However, when the kinetics is coupled to a fast bath, the arrival time distribution narrows (loss of memory) and arrival times become short. This *time domain* effect is quite similar to motional narrowing in the *frequency domain*.

The joint distributions of arrival times allows to study dynamics of correlations of bath variables. First, asym-

metry of contour plots implies asymmetic bath evolution paths, which in turn implies inequivalence of kinetic rates associated with different bath state channels. Second, change in the amplitude (shape) of the two-dimensional surfaces (of contour lines in the contour plots) for $q_{b\alpha}(\tau_1,\tau_2;t)$, $q_{b\beta}(\tau_1,\tau_2;t)$ as well as the ensemble average quantity $\langle Q(\tau_1,\tau_2;t)\rangle$ for different separation times t_1 and t_2 signifies a presence of bath correlations. As these correlations decay, the amplitude decreases (contour lines change from convex out to convex in when viewed along the diagonal $\tau_1=\tau_2$). n-point experiments considered here, can also be employed to study lineshape fluctuations.[25]

Finally we show how to use the one- and two-point distributions of photon arrival times $\mathbf{Q}(\tau_1)$ and $\mathbf{Q}(\tau_1,\tau_2;t)$ to probe the characteristic bath evolution timescale. Using the factorization (17) for the conditional probability $\mathbf{Q}(\tau_1,\tau_2;t)$, expression (20) for $\langle Q(\tau_1,\tau_2;t)\rangle$ and algebra of the matrices $\mathbf{G}^{\mathrm{eq}}$ and $\mathbf{G}^{neq}$ presented in Appendix A, we obtain

$$S(t_1,t_2)\equiv\frac{\langle Q(\tau_1,\tau_2;t_2)\rangle-\langle Q(\tau_2)\rangle\langle Q(\tau_1)\rangle}{\langle Q(\tau_1,\tau_2;t_1)\rangle-\langle Q(\tau_2)\rangle\langle Q(\tau_1)\rangle}=\exp[-R(t_2-t_1)], \tag{27}$$

Eq. (27) is valid for the two-state jump model of the bath, arbitrary number of protein sites $(A,B,\ldots)$ partaking in excitation transfer and a wide range of the relevant time scales. Equation (27) contains average quantities accessible from the experimental one- and two-point histograms of the photon arrival times. Therefore, using the average distribution of arrival times $\langle Q(\tau_1)\rangle$ obtained from one-point measurement PAT data and the average joint distributions $\langle Q(\tau_1,\tau_2;t_1)\rangle$ and $\langle Q(\tau_1,\tau_2;t_2)\rangle$ obtained from two-point measurement PAT data for only two interphoton separation times $t_2>t_1$, we can find the bath time scale R. We have verified the validity of Eq. (27) by computing the ratio $S(t_1,t_2)$ for short $t_1=1.0$ μs and long $t_2=10.0$ μs separation times and values of arrival times τ_1 and τ_2 corresponding to maximum of $\langle Q(\tau)\rangle$ for models $M9-M11$ and obtained a good agreement between R used in simulation of one- and two-point measurement and the value of R obtained from Eq. (27).

ACKNOWLEDGMENTS

The support of the U.S. Department of Energy, Office of Basic Energy Sciences, Chemical Sciences Division DE-FG02-01ER15155 and the Petroleum Research Fund administered by the American Chemical Society is gratefully acknowledged. We also wish to thank Professor Sunney Xie for most useful discussions.

APPENDIX A: GREEN FUNCTIONS FOR THE MULTI-STATE BATH EVOLUTION

In this section we derive the propagator $G(t)$ for two-state jump bath used in Eq. (17). In the n-state model of the bath the dynamics of a bath variable X is described by the master equation

$$\dot{w}_i(t)=\sum_{i,j} R_{ji}w_j(t)-R_{ij}w_i(t), \tag{A1}$$

where w_i, $i=1,2,\ldots n$ denote the probability density of X to be in state $X_1,X_2,\ldots,X_n$ respectively; R_{ij}, are the rate constants for interconversion from state i to state j. We solve Eqs. (A1) by recasting it into a matrix form

$$\dot{\mathbf{W}}(t)=\mathbf{R}\mathbf{W}(t), \tag{A2}$$

where $R_{ij}=R_{ij}$ and $R_{ii}=-\Sigma_{i\neq j}R_{ji}$. To calculate the probability density $\mathbf{W}(t_1)$ at time t_1, given the probability density is $\mathbf{W}(t_0)$ at time t_0, we define the conditional probability density matrix

$$\mathbf{G}(t_1,t_0)=\mathbf{G}(t_1-t_0,0)=\mathbf{G}(t). \tag{A3}$$

Then, $\mathbf{W}(t)$ can be computed as

$$\mathbf{W}(t)=\mathbf{G}(t)\mathbf{W}(0), \tag{A4}$$

and $\mathbf{G}(t)$ is governed by the same master equations (A2) that govern $\mathbf{W}(t)$, i.e.,

$$\dot{\mathbf{G}}(t)=\mathbf{R}\mathbf{G}(t), \tag{A5}$$

Eq. (A5) can be solved in the Laplace domain as

$$\tilde{\mathbf{G}}(s)=(s\mathbf{I}-\mathbf{R})^{-1}. \tag{A6}$$

Solving for the two-state model (see Fig. 2) with a kinetic rate matrix given by Eqs. (4), we obtain matrix $\mathbf{G}(t)$ by inverse Laplace transformation

$$\mathbf{G}(t)=(\mathbf{G}^{\mathrm{eq}}+\mathbf{G}^{neq}e^{-Rt}), \tag{A7}$$

where $R=R_{\alpha\beta}+R_{\beta\alpha}$ and the 2×2 matrices $\mathbf{G}^{\mathrm{eq}}$ and $\mathbf{G}^{neq}$ are given by

$$\mathbf{G}^{\mathrm{eq}}=R^{-1}\begin{pmatrix}R_{\alpha\beta} & R_{\alpha\beta}\\ R_{\beta\alpha} & R_{\beta\alpha}\end{pmatrix},$$

and

$$\mathbf{G}^{neq}=R^{-1}\begin{pmatrix}R_{\beta\alpha} & -R_{\alpha\beta}\\ -R_{\beta\alpha} & R_{\alpha\beta}\end{pmatrix}. \tag{A8}$$

Note that $\mathbf{G}^{\mathrm{eq}}$ and $\mathbf{G}^{neq}$ are orthogonal and idempotent matrices, i.e.,

$$\mathbf{G}^{\mathrm{eq}}\mathbf{G}^{neq}=\mathbf{G}^{neq}\mathbf{G}^{\mathrm{eq}}=\mathbf{0},\quad \mathbf{G}^{\mathrm{eq}}\mathbf{G}^{\mathrm{eq}}=\mathbf{G}^{\mathrm{eq}},\quad \mathbf{G}^{neq}\mathbf{G}^{neq}=\mathbf{G}^{neq}, \tag{A9}$$

where $\mathbf{0}$ is a 2×2 matrix with zero entrees, and

$$\mathbf{G}^{\mathrm{eq}}+\mathbf{G}^{neq}=\mathbf{0}. \tag{A10}$$

The equilibrium population vector $\mathbf{w}^{\mathrm{eq}}$ is an eigenstate of $\mathbf{G}^{\mathrm{eq}}$ with the unit eigenvalue and in the kernel of $\mathbf{G}^{neq}$

$$\mathbf{G}^{\mathrm{eq}}\mathbf{w}^{\mathrm{eq}}=\mathbf{w}^{\mathrm{eq}},\quad \mathbf{G}^{neq}\mathbf{w}^{\mathrm{eq}}=\overline{0}, \tag{A11}$$

where $\overline{0}$ a zero column vector.

APPENDIX B: LIMITING CASES FOR k, K, AND R

In this section we present expressions for the elements of conditional distribution matrix $\mathbf{Q}(\tau_1)=\{Q(\tau_1)\}_{ij}$ defined in Eq. (11) for limiting cases I–IV discussed in Sec. IV.

Case I: Off-diagonal terms $Q_{b\alpha,a\beta}$ and $Q_{b\beta,a\alpha}$ are negligible and

$$Q_{b\alpha,a\alpha}(\tau_1)=k_bK^{\alpha}_{ab}\frac{e^{-z^{\alpha}_1\tau_1}-e^{-z^{\alpha}_2\tau_1}}{(z^{\alpha}_2-z^{\alpha}_1)},$$
$$Q_{b\beta,a\beta}(\tau_1)=k_bK^{\beta}_{ab}\frac{e^{-z^{\beta}_1\tau_1}-e^{-z^{\beta}_2\tau_1}}{(z^{\beta}_2-z^{\beta}_1)}, \tag{B1}$$

where

$$z^{\alpha}_{1,2}=\tfrac{1}{2}[k_b\pm\sqrt{k_b^2-2k_b(K^{\alpha}_{ba}-K^{\alpha}_{ab})}],$$
$$z^{\beta}_{1,2}=\tfrac{1}{2}[k_b\pm\sqrt{k_b^2-2k_b(K^{\beta}_{ba}-K^{\beta}_{ab})}]. \tag{B2}$$

Case II: As in case I, the diagonal terms of $\mathbf{Q}(\tau_1)$ are given by same Eqs. (B1) with

$$z^{\alpha}_{1,2}=\tfrac{1}{2}[K^{\alpha}_{ab}+K^{\alpha}_{ba}\pm\sqrt{(K^{\alpha}_{ab}+K^{\alpha}_{ba})^2-2k_b(K^{\alpha}_{ba}-K^{\alpha}_{ab})}],$$
$$z^{\beta}_{1,2}=\tfrac{1}{2}[K^{\beta}_{ab}+K^{\beta}_{ba}\pm\sqrt{(K^{\beta}_{ab}+K^{\beta}_{ba})^2-2k_b(K^{\beta}_{ba}-K^{\beta}_{ab})}]. \tag{B3}$$

Case III:

$$Q_{b\alpha,a\alpha}(\tau_1)=k_b\left(\frac{K^{\alpha}_{ab}(z_1-R_{\beta\alpha}-K^{\beta}_{ab})(e^{-z_1\tau_1}-e^{-k_b\tau_1})}{(k_b-z_1)(z_1-z_2)}-\frac{K^{\alpha}_{ab}(z_2-R_{\beta\alpha}-K^{\beta}_{ab})(e^{-z_2\tau_1}-e^{-k_b\tau_1})}{(k_b-z_2)(z_1-z_2)}\right),$$
$$Q_{b\alpha,a\beta}(\tau_1)=k_b\left(\frac{K^{\alpha}_{ab}R_{\beta\alpha}(e^{-z_2\tau_1}-e^{-k_b\tau_1})}{(k_b-z_2)(z_1-z_2)}-\frac{K^{\alpha}_{ab}R_{\beta\alpha}(e^{-z_1\tau_1}-e^{-k_b\tau_1})}{(k_b-z_1)(z_1-z_2)}\right),$$
$$Q_{b\beta,a\alpha}(\tau_1)=k_b\left(\frac{K^{\beta}_{ab}(z_1-R_{\alpha\beta}-K^{\alpha}_{ab})(e^{-z_1\tau_1}-e^{-k_b\tau_1})}{(k_b-z_1)(z_1-z_2)}-\frac{K^{\beta}_{ab}(z_2-R_{\beta\alpha}-K^{\alpha}_{ab})(e^{-z_2\tau_1}-e^{-k_b\tau_1})}{(k_b-z_2)(z_1-z_2)}\right),$$
$$Q_{b\beta,a\beta}(\tau_1)=k_b\left(\frac{K^{\beta}_{ab}R_{\alpha\beta}(e^{-z_2\tau_1}-e^{-k_b\tau_1})}{(k_b-z_2)(z_1-z_2)}-\frac{K^{\beta}_{ab}R_{\alpha\beta}(e^{-z_1\tau_1}-e^{-k_b\tau_1})}{(k_b-z_1)(z_1-z_2)}\right), \tag{B4}$$

where

$$z_{1,2}=\tfrac{1}{2}[(R_{\alpha\beta}+R_{\beta\alpha})\pm\sqrt{(R_{\alpha\beta}+R_{\beta\alpha})+2(R_{\alpha\beta}-R_{\beta\alpha})(K^{\alpha}_{ab}-K^{\beta}_{ab})}]. \tag{B5}$$

Case IV:

$$Q_{b\alpha,a\alpha}(\tau_1)=k_be^{-k_b\tau_1}\left(\frac{R_{\beta\alpha}+R_{\alpha\beta}e^{-(R_{\beta\alpha}+R_{\alpha\beta})\tau_1}}{R_{\beta\alpha}+R_{\alpha\beta}}\right)\times\left(\frac{K^{\alpha}_{ab}-K^{\alpha}_{ab}e^{-(K^{\alpha}_{ab}+K^{\alpha}_{ba})\tau_1}}{K^{\alpha}_{ab}+K^{\alpha}_{ba}}\right),$$
$$Q_{b\alpha,a\beta}(\tau_1)=k_be^{-k_b\tau_1}\left(\frac{R_{\beta\alpha}-R_{\beta\alpha}e^{-(R_{\beta\alpha}+R_{\alpha\beta})\tau_1}}{R_{\beta\alpha}+R_{\alpha\beta}}\right)\times\left(\frac{K^{\beta}_{ab}-K^{\beta}_{ab}e^{-(K^{\beta}_{ab}+K^{\beta}_{ba})\tau_1}}{K^{\beta}_{ab}+K^{\beta}_{ba}}\right),$$
$$Q_{b\beta,a\alpha}(\tau_1)=k_be^{-k_b\tau_1}\left(\frac{R_{\alpha\beta}-R_{\alpha\beta}e^{-(R_{\beta\alpha}+R_{\alpha\beta})\tau_1}}{R_{\beta\alpha}+R_{\alpha\beta}}\right)\times\left(\frac{K^{\alpha}_{ab}-K^{\alpha}_{ab}e^{-(K^{\alpha}_{ab}+K^{\alpha}_{ba})\tau_1}}{K^{\alpha}_{ab}+K^{\alpha}_{ba}}\right),$$
$$Q_{b\beta,a\beta}(\tau_1)=k_be^{-k_b\tau_1}\left(\frac{R_{\alpha\beta}+R_{\beta\alpha}e^{-(R_{\beta\alpha}+R_{\alpha\beta})\tau_1}}{R_{\beta\alpha}+R_{\alpha\beta}}\right)\times\left(\frac{K^{\beta}_{ab}-K^{\beta}_{ab}e^{-(K^{\beta}_{ab}+K^{\beta}_{ba})\tau_1}}{K^{\beta}_{ab}+K^{\beta}_{ba}}\right). \tag{B6}$$

[1] T. Plakhotnik, E. A. Donley, and U. P. Wild, Annu. Rev. Phys. Chem. **48**, 181 (1997).
[2] "Spectroscopy of Single Molecules in Physics, Chemistry and Life Sciences" Chem. Phys. **247**, 1 (1999); J. Wang and P. Wolynes, Phys. Rev. Lett. **74**, 4317 (1995).
[3] X. S. Xie and J. K. Trautman, Annu. Rev. Phys. Chem. **49**, 441 (1998).
[4] X.-H. Xu and E. S. Young, Science **275**, 1066 (1997); R. M. Dickson, D. J. Norris, Y.-L. Tzeng, and W. E. Moerner, **274**, 966 (1966).
[5] H.-P. Lu and X. S. Xie, Nature (London) **385**, 143 (1997); **49**, 441 (1998); H. P. Lu, L. Xun and X. S. Xie, Science **282**, 1877 (1998).
[6] S. Wennmaim, L. Edman, and R. Rigler, Proc. Natl. Acad. Sci. U.S.A. **94**, 10641 (1997).
[7] V. Chernyak, M. Schulz, and S. Mukamel, J. Chem. Phys. **111**, 7416 (1999).
[8] E. W. Schlag, S.-Y. Sheu, D.-Y. Yang, H. L. Selzle, and S. H. Lin, Proc. Natl. Acad. Sci. U.S.A. **97**, 1068 (2000); E. W. Schlag, S. H. Lin, R. Weinkauf, and P. M. Rentsepis, *ibid.*, **95**, 1358 (1998).
[9] R. Weinkauf, P. Aicher, G. Wesley, J. Grotemeyer, and E. W. Schlag, J. Phys. Chem. **98**, 8381 (1994); R. Weinkauf, P. Schanen, D. Yang, S. Soukara, and E. W. Schlag, *ibid.*, **99**, 11255 (1995).
[10] X. Zhuang, T. Ha, H. D. Kim, T. Centner, S. Labeit, and S. Chu, Proc. Natl. Acad. Sci. U.S.A. **97**, 14241 (2000).
[11] J. Wang, J. Onuchic, and P. Wolynes, Phys. Rev. Lett. **76**, 4861 (1996); J. N. Onuchic, J. Wang, and P. Wolunes, Chem. Phys. **247**, 175 (1999).
[12] L. Fleury, J.-K. Segura, G. Zumofen, B. Hecht, and U. P. Wild, Phys. Rev. Lett. **84**, 1148 (2000).
[13] L. Fleury, A. Zambusch, M. Orrit, R. Brown, and J. Bernard, J. Lumin. **56**, 15 (1993).
[14] A.-M. Boiron, Ph. Tamarat, B. Lounis, R. Brown, and M. Orrit, Chem. Phys. **247**, 119 (1999).
[15] A. Zambusch, L. Fleury, R. Brown, J. Bernard, and M. Orrit, Phys. Rev. Lett. **70**, 3584 (1993).
[16] R. Kettner, J. Tittel, Th. Basche, and C. Brauchle, J. Phys. Chem. **98**, 6671 (1994).
[17] J. Tittel, R. Kettner, Th. Basche, C. Brauchle, H. Quante, and K. Mullen, J. Lumin. **64**, 1 (1995).
[18] B. Kozankiewicz, J. Bernard, and M. Orrit, J. Chem. Phys. **101**, 9377 (1994).
[19] H. Yang and X. Sunney Xie, J. Chem. Phys. (unpublished); H. Yang and X. Sunney Xie, Chem. Phys. (unpublished).
[20] E. Geva and J. L. Skinner, Chem. Phys. Lett. **288**, 225 (1998).
[21] S. Yang and J. Cao, J. Phys. Chem. B **105**, 6536 (2001).
[22] A. M. Berezhkovskii, A. Szabo, and G. H. Weiss, J. Chem. Phys. **110**, 9145 (1999); A. M. Berezhkovskii, A. Szabo, and G. H. Weiss, J. Phys. Chem. B **104**, 3776 (2000).
[23] T. Ha, Th. Enderle, D. F. Ogletree, D. S. Chemla, P. R. Selvin, and S. Weiss, Proc. Natl. Acad. Sci. U.S.A. **93**, 6264 (1996).
[24] P. D. Reilly and J. L. Skinner, Phys. Rev. Lett. **71**, 4257 (1993); P. D. Reilly and J. L. Skinner, J. Chem. Phys. **101**, 965 (1994).

[25] E. Barkai, Y.-J. Jung, and R. Silbey, Phys. Rev. Lett. **87**, 207403 (2001).
[26] E. Barkai, R. Silbey, and G. Zumofen, Phys. Rev. Lett. **84**, 5339 (2000); E. Barkai, R. Silbey, and G. Zumofen, J. Chem. Phys. **113**, 5853 (2000).
[27] E. Geva and J. L. Skinner, J. Phys. Chem. B **101**, 8920 (1997).
[28] P. W. Anderson, J. Phys. Soc. Jpn. **9**, 316 (1954); P. W. Anderson, B. I. Halperin, and C. M. Varma, Philos. Mag. **25**, 1 (1971).
[29] R. Kubo, J. Phys. Soc. Jpn. **6**, 935 (1954); R. Kubo, Adv. Chem. Phys. **15**, 101 (1969).
[30] Y. Zhao, V. Chernyak, and S. Mukamel, J. Phys. Chem. A **102**, 6614 (1998).
[31] L. Mandel and E. Wolf, *Optical Coherence and Quantum Optics* (Cambridge University Press, New York, 1995).
[32] C. Eggeling, J. R. Fries, L. Brand, R. Guenter, and C. A. M. Seidel, Proc. Natl. Acad. Sci. U.S.A. **95**, 1556 (1998); J. Tellinghuisen, P. M. Goodwin, W. P. Ambrose, J. C. Martin, and P. M. Keller, Anal. Chem. **66**, 64 (1994).
[33] S. Mukamel, *Principles of Nonlinear Optical Spectroscopy* (Oxford, New York, 1995).
[34] V. Barsegov and S. Mukamel, J. Chem. Phys. **116**, 9802 (2002).
[35] V. Barsegov, V. Chernyak, and S. Mukamel, J. Chem. Phys. **116**, 4240 (2002).
[36] R. Kubo, J. Math. Phys. **4**, 174 (1963).
[37] R. Kubo, M. Toda, and N. Hashitsume, *Statistical Physics, Vol. 2: Non-Equilibrium Statistical Mechanics* (Springer-Verlag, Berlin, 1995).
[38] P. Lancaster and M. Tismenetsky, *The Theory of Matrices: 2nd ed. with Applications*, (Academic, New York, 1985).